Proceedings of ASME 2014 International Mechanical Engineering Congress & Exposition
IMECE 2014
November 14-20, 2014, Montreal, Canada

IMECE2014-36082

ENHANCEMENT OF FREE VORTEX FILAMENT METHOD FOR AERODYNAMIC LOADS ON ROTOR BLADES

Hamidreza Abedi
Division of Fluid Dynamics
Department of Applied Mechanics
Chalmers University of Technology
Göteborg, Sweden
Email: abedih@chalmers.se

Lars Davidson
Division of Fluid Dynamics
Department of Applied Mechanics
Chalmers University of Technology
Göteborg, Sweden
Email: lada@chalmers.se

Spyros Voutsinas
Fluid Section
School of Mechanical Engineering
National Technical University of Athens
Athens, Greece
spyros@fluid.mech.ntua.gr

ABSTRACT

The aerodynamics of a wind turbine is governed by the flow around the rotor, where the prediction of air loads on rotor blades in different operational conditions and its relation to rotor structural dynamics is one of the most important challenges in wind turbine rotor blade design. Because of the unsteady flow field around wind turbine blades, prediction of aerodynamic loads with high level of accuracy is difficult and increases the uncertainty of load calculations.

A free vortex wake method, based on the potential, inviscid and irrotational flow, is developed to study the aerodynamic loads. Since it is based on the potential, inviscid and irrotational flow, it cannot be used to predict viscous phenomena such as drag and boundary layer separation. Therefore it must be coupled to the tabulated airfoil data to take the viscosity effects into account. The results are compared with the Blade Element Momentum (BEM) [1] method and the GENUVP code [2] (see also the acknowledgments).

NOMENCLATURE

h Perpendicular distance
t time
c Airfoil chord
K_v Correction factor
C_L Lift coefficient
α Angle of attack
$\vec{V}_{tot}$ Total velocity vector
$\vec{V}_{ind}$ Induced velocity vector
Γ Circulation
$\vec{r}$ Position vector
r_{core} Vortex core radius
$\vec{V}_{\infty}$ Upstream flow velocity vector
Ω Rotational velocity
$\vec{n}$ Normal unit vector
$\vec{L}$ Lift force
$\vec{D}$ Drag force
$\vec{L'}$ Lift force per blade span
$\vec{F_t}$ Tangential force
$\vec{F_n}$ Normal force
α_0 Zero lift angle of attack
ρ Air density
γ Vorticity distribution
C_D Drag coefficient

INTRODUCTION

The methods for predicting wind turbine performance are similar to propeller and helicopter theories. There are different methods for modelling the aerodynamics of a wind turbine with different levels of complexity and accuracy, such as the BEM theory and solving the Navier-Stokes equations using CFD.

The vortex theory, which is based on the potential, inviscid and irrotational flow, can also be used to predict the aerodynamic performance of wind turbines. It has been widely used for aerodynamic analysis of airfoils and aircrafts. Although the standard

Copyright © 2014 by ASME

method cannot be used to predict viscous phenomena such as drag and boundary layer separation, its combination with tabulated airfoil data makes it a powerful tool for the prediction of fluid flow. Compared with the BEM method, the vortex method is able to provide more physical solutions for attached flow conditions using boundary layer corrections, and it is also valid over a wider range of turbine operating conditions. Although it is computationally more expensive than the BEM method, it is still feasible as an engineering method.

In vortex methods, the trailing and shed vortices are modeled by either vortex particles or vortex filaments moving either freely, known as free wake [2–4] or restrictedly by imposing the wake geometry, known as prescribed wake [5, 6]. The prescribed wake requires less computational effort than the free wake, but it requires experimental data to be valid for a broad range of operating conditions. The free wake model, which is the most computationally expensive vortex method, is able to predict the wake geometry and loads more accurately than the prescribed wake because of less restrictive assumptions. Therefore, it can be used for the load calculations, especially for the unsteady flow environment. However, its application is limited to the attached flow and it must be linked to the tabulated airfoil data to predict the air loads in the presence of the drag and the flow separation.

Wind turbines always operate in the unsteady flow condition. The unsteadiness sources are classified according to the atmospherical conditions, e.g. wind shear, turbulent inflow and wind gusts together with the turbine structure such as yaw misalignment, rotor tilt and blade elastic deformation [7] which are considered as perturbations of the local angle of attack and the velocity field. Since the variation in frequency of these sources may be high, the quasi-static aerodynamic is no longer valid [8, 9]. As a consequence, a dynamic approach must be introduced to modify the aerodynamic coefficients for unsteady operating conditions. This approach which is called Dynamic Stall, adjusts the lift, the drag and the moment coefficients for each blade element on the basis of the 2D static airfoil data together with the correction for the separated flow.

In steady flow, when the angle of attack for some blade regions exceeds from the critical angle of attack (α_{stall}), which is equivalent to the maximum lift coefficient ($C_{L,max}$), the flow is separated. This phenomenon is called static stall. This phenomenon, for an airfoil in unsteady flow, is associated with so-called dynamic stall where its major effect is stall delay and an excessive force (see Fig.(1)). In other words, when an airfoil or a lifting surface is exposed to time-varying pitching, plunging and incident velocity, the stall condition happens at an angle of attack higher than the static stall angle which means that the flow is separated at a higher angle of attack than in steady flow. When stall occurs there is a sudden decrease in lift. By decreasing the angle of attack, the flow re-attaches again (stall recovery), but at a lower angle than the static stall angle [10]. This scenario, which is called dynamic stall, occurs around the stall angle and the result is hysteresis loops and a sudden decrease of the lift coefficient. Hence, the dynamic stall describes a series of event resulting in dynamic delay of stall to angles above the static stall angle and it provides the unsteady evolution of lift, drag and moment coefficients along the rotor blade. Because of the dynamic stall, the predicted aerodynamic coefficients may result in noticeable errors [8] in comparison with the static ones.

Although the unsteady aerodynamics is mostly referred to the dynamic stall, but it might be generated on the lifting surfaces even in the absence of the dynamic stall [8], a dynamic stall model for the unsteady aerodynamic loads prediction is therefore crucial for the wind turbine technology development. In this paper, an in-house time-marching vortex lattice free wake is used for the simulation where its potential solution is coupled to the tabulated airfoil data for the wind turbine load calculation. In addition, a semi-empirical model, called Extended ONERA model is added to account for the dynamic stall effects. The results using the three different free vortex methods are compared, namely standard potential method, 2D static airfoil data model and the dynamic stall model.

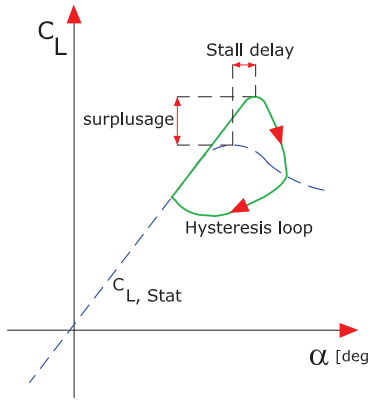

FIGURE 1. HYSTERESIS LOOP AROUND THE STALL ANGLE

Theory

Vortex flow theory is based on assuming incompressible ($\nabla \cdot \vec{V} = 0$) and irrotational ($\nabla \times \vec{V} = 0$) flow at every point except at the origin of the vortex, where the velocity is infinite [11]. A region containing a concentrated amount of vorticity is called a vortex, where a vortex line is defined as a line whose tangent is parallel to the local vorticity vector everywhere. Vortex lines surrounded by a given closed curve make a vortex tube with a strength equal to the circulation Γ. A vortex filament with a strength of Γ, is represented as a vortex tube of an infinitesimal cross-section with strength Γ.

Copyright © 2014 by ASME

According to the Helmholtz theorem, an irrotational motion of an inviscid fluid which started from rest remains irrotational. Also, a vortex line cannot end in the fluid. It must form a closed path, end at a solid boundary or go to infinity; this implies that vorticity can only be generated at solid boundaries. Therefore, a solid surface may be considered as a source of vorticity. Hence the solid surface in contact with fluid is replaced by a distribution of vorticity.

For an irrotational flow, a velocity potential, Φ, can be defined as $\vec{V} = \nabla\Phi$, where in order to find the velocity field, the Laplace's equation, $\nabla^2\Phi = 0$, is solved using a proper boundary condition for the velocity on the body and at infinity. In addition, in vortex theory, the vortical structure of a wake can be modeled by either vortex filaments or vortex particles, where a vortex filament is modeled as concentrated vortices along an axis with a singularity at the center.

The velocity induced by a straight vortex filament can be determined by the Biot-Savart law as

$$\vec{V}_{ind} = \frac{\Gamma}{4\pi}\frac{\vec{dl}\times\vec{r}}{|\vec{r}|^3} \tag{1}$$

which can also be written as

$$\vec{V}_{ind} = \frac{\Gamma}{4\pi}\frac{(r_1+r_2)(\vec{r}_1\times\vec{r}_2)}{(r_1r_2)(r_1r_2+\vec{r}_1\cdot\vec{r}_2)} \tag{2}$$

where Γ denotes the strength of the vortex filament and $\vec{r_1}$, $\vec{r_2}$ are the distance vectors from the beginning, A, and end, B, of a vortex segment to an arbitrary point C, respectively (see Fig.(2)).

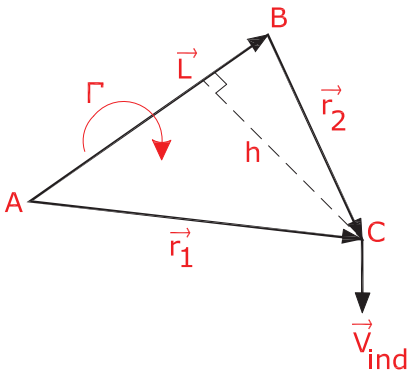

FIGURE 2. SCHEMATIC FOR THE BIOT-SAVART LAW

The Biot-Savart law has a singularity when the point of evaluation (C) of induced velocity is located on the vortex filament axis ($\vec{L}$). Also, when the evaluation point is very near to the vortex filament, there is an unphysically large induced velocity at that point. The remedy is either to use a cut-off radius, δ [12], or to use a viscous vortex model with a finite core size by multiplying a factor to remove the singularity [13].

The Biot-Savart law correction based on the viscous vortex model can be made by introducing a finite core size, r_c, for a vortex filament [14].

Here, for simplicity, a constant viscous core size model, which is one of the general approaches using desingularized algebraic profile, is applied for the induced velocity calculations. A general form of a desingularized algebraic swirl-velocity profile for stationary vortices is proposed by Vasitas [15] as

$$V_\theta(r) = \frac{\Gamma}{2\pi}\left(\frac{r}{(r_c^{2n}+r^{2n})^{1/n}}\right) \tag{3}$$

Bagai [16] suggested the velocity profile based on Eq.(3) for $n = 2$ for the rotor tip vortices. Therefore, in order to take into account the effect of viscous vortex core, a factor of K_v must be added to the Biot-Savart law as [16]

$$\vec{V}_{ind} = K_v\frac{\Gamma}{4\pi}\frac{(r_1+r_2)(\vec{r}_1\times\vec{r}_2)}{(r_1r_2)(r_1r_2+\vec{r}_1\cdot\vec{r}_2)} \tag{4}$$

where

$$K_v = \frac{h^n}{(r_c^{2n}+h^{2n})^{1/n}} \tag{5}$$

and h is defined as the perpendicular distance of the evaluation point (see Fig.(2)).

Factor K_v desingularizes the Biot-Savart equation when the evaluation point distance tends to zero and prevents a high induced velocity in the vicinity region of the vortex core radius.

Assumptions

Each engineering model is constructed based on some assumptions. Here, some of those are discussed. The upstream flow is set to be uniform, both in time and space, and is perpendicular to the rotor plane (parallel to the rotating axis). However, it can be either uniform or non-uniform (varying both in time and space). Blades are assumed to be rigid, so the elastic effect of the blades is neglected. Because of the large circulation gradients ($d\Gamma/dr$) near the tip and the root of the rotor blade, the cosine rule for the blade radial segmentation [17] is used where the blade elements, in the chordwise direction, are distributed at equi-distant increments.

Copyright © 2014 by ASME

In the vortex lattice free wake model, a finite number of vortex wake elements move freely based on the local velocity field, and contrary to the prescribed wake model, allowing wake expansion as well. Each vortex wake element contains two points, one at the head (A), and another at the tail (B) (see Fig.(2)), which are known as Lagrangian markers, where the induced velocity components are calculated using the Biot-Savart law; their movements give rise to the wake deformation. The vortex flow theory assumes that the trailing and shed wake vortices extend to infinity. However, since the effect of the induced velocity field by the far wake is small on the rotor blade, the wake in the present study extends only to four diameters downstream of the wind turbine rotor plane.

Vortex Lattice Free Wake (VLFW)

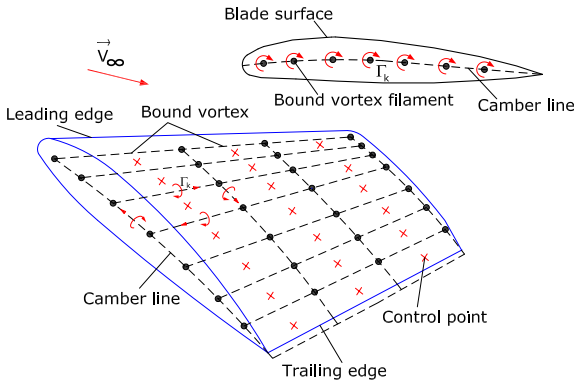

FIGURE 3. LIFTING SURFACE AND VORTEX PANELS CONSTRUCTION

The vortex lattice method (VLM) is based on the thin lifting surface theory of vortex ring elements [18], where the blade surface is replaced by vortex panels that are constructed based on the airfoil camber line of each blade section (see Fig.(3)). The solution of Laplace's equation with a proper boundary condition gives the flow around the blade resulting in an aerodynamic load calculation, generated power and thrust of the wind turbine. To take the blade surface curvature into account, the lifting surface is divided into a number of panels both in the chordwise and spanwise directions, where each panel contains a vortex ring with strength $\Gamma_{i,j}$ in which i and j indicate panel indices in the chordwise and spanwise directions, respectively. The strength of each blade bound vortex ring element, $\Gamma_{i,j}$, is assumed to be constant over the panel and the positive circulation is defined on the basis of right-hand rotation rule. In order to fulfill the 2D Kutta condition (which can be expressed as $\gamma_{T.E.} = 0$ in terms of the strength of the vortex sheet) the leading segment of a vortex ring is located at the $1/4$ panel length (see Fig.(5)). The control point

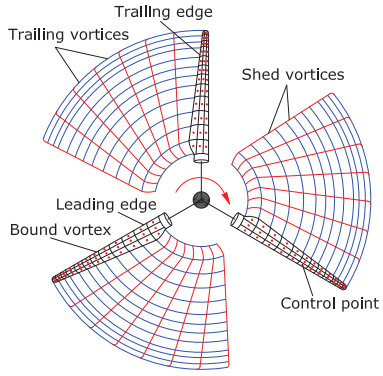

FIGURE 4. SCHEMATIC OF VORTEX LATTICE FREE WAKE

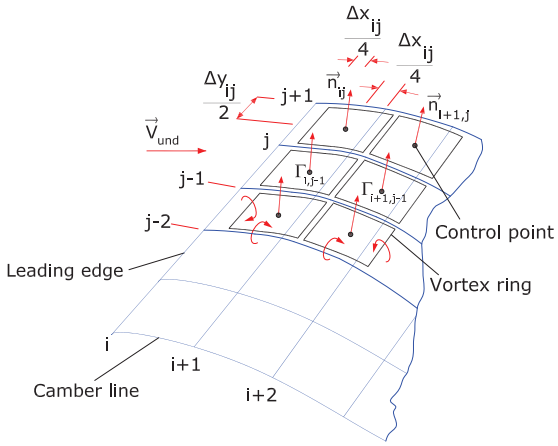

FIGURE 5. NUMBERING PROCEDURE

of each panel is located at $3/4$ of the panel length meaning that the control point is placed at the center of the panel's vortex ring.

Generally, the wake vortices are modeled as vortex ring elements that are trailed and shed, based on the time-marching method, from the trailing edge; in the wake they induce a velocity field around the blade.

To find the blade bound vortices' strength, the flow tangency condition at each blade control point must be specified by establishing a system of equations. Therefore, the normal vector at each control point must be defined (see Fig.(5)). The velocity components at each blade control point includes the free stream ($\vec{V}_\infty$), rotational ($\Omega\vec{r}$), blade vortex rings self-induced ($\vec{V}_{ind,bound}$) and wake induced ($\vec{V}_{ind,wake}$) velocities. The blade induced component is known as influence coefficient a_{ij} and is defined as the induced velocity of a j^{th} blade vortex ring with a strength equal to one on the i^{th} blade control point given by

$$a_{ij} = \left(\vec{V}_{ind,bound}\right)_{ij} \cdot \vec{n}_i \qquad (6)$$

Copyright © 2014 by ASME

If the blade is assumed to be rigid, then the influence coefficients are constant at each time step, which means that the left-hand side of the equation system is computed only once. However, if the blade is modeled as a flexible blade, they must be calculated at each time step. Since the wind and rotational velocities are known during the wind turbine operation, they are transferred to the right-hand side of the equation system. In addition, at each time step, the strength of the wake vortex panels is known from the previous time step, so the induced velocity contribution by the wake panels is also transferred to the right-hand side. Therefore, the system of equations can be expressed as

$$\begin{pmatrix} a_{11} & a_{12} & \cdots & a_{1m} \\ a_{21} & a_{22} & \cdots & a_{2m} \\ \vdots & \vdots & \ddots & \vdots \\ a_{m1} & a_{m2} & \cdots & a_{mm} \end{pmatrix} \begin{pmatrix} \Gamma_1 \\ \Gamma_2 \\ \vdots \\ \Gamma_m \end{pmatrix} = \begin{pmatrix} RHS_1 \\ RHS_2 \\ \vdots \\ RHS_m \end{pmatrix} \tag{7}$$

where m is defined as $m = M \times N$ for a blade with M spanwise and N chordwise panels and the right-hand side is computed as

$$RHS_k = -\left(\vec{V}_\infty + \Omega\vec{r} + \vec{V}_{ind,wake}\right)_k \cdot \vec{n}_k \tag{8}$$

The blade bound vortex strength ($\Gamma_{i,j}$) is calculated by solving Eq.(7) at each time step. At the first time step (see Fig.(6) and (7)), there are no free wake elements. At the second time step (see Fig.(6) and (8)), when the blade is rotating, the first wake panels are shed. Their strength is equal to the bound vortex circulation of the last row of the blade vortex ring elements (Kutta condition), located at the trailing edge, at the previous time step (see Fig.(6)), which means that $\Gamma_{W_{t_2}} = \Gamma_{T.E.,t_1}$, where the W and $T.E.$ subscripts represent the wake and the trailing edge, respectively. At the second time step, the strength of the blade bound vortex rings is calculated by specifying the flow tangency boundary condition where, in addition to the blade vortex ring elements, the contribution of the first row of the wake panels is considered.

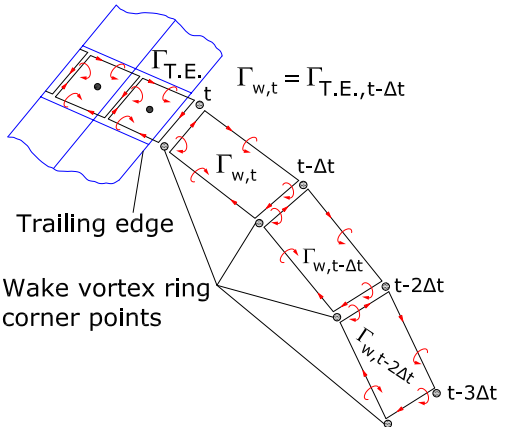

FIGURE 6. SCHEMATIC OF GENERATION AND MOVING OF WAKE PANELS AT EACH TIME STEP

This methodology is repeated, and the vortex wake elements are trailed and shed at each time step, where their strengths remain constant (Kelvin theorem) and their corner points are moved based on the governing equation (Eq.(9)) by the local velocity field, including the wind velocity and the induced velocity by all blade and wake vortex rings (see Fig.(7) and (8)).

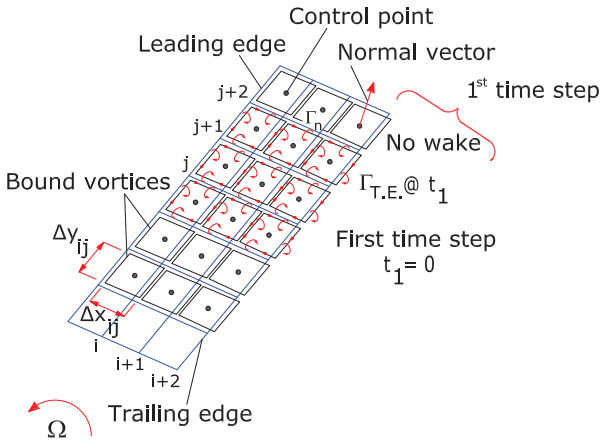

FIGURE 7. SCHEMATIC OF WAKE EVOLUTION AT THE FIRST TIME STEP

The governing equation for the wake geometry is

$$\frac{d\vec{r}}{dt} = \vec{V}(\vec{r},t) \qquad \vec{r}(t=0) = \vec{r_0} \tag{9}$$

where $\vec{r}$, $\vec{V}$ and t denote the position vector of a Lagrangian marker, the total velocity field and time, respectively, and the total velocity field, expressed in the rotating reference frame i.e., $\vec{V}_{rot} = 0$, can be written as

$$\vec{V} = \vec{V}_\infty + \vec{V}_{ind,bound} + \vec{V}_{ind,wake} \tag{10}$$

Different numerical schemes may be used for Eq.(9) such as the explicit Euler method, the implicit method, the Adams-Bashforth method and the Predictor-Corrector method. The numerical integration scheme must be considered in terms of the

Copyright © 2014 by ASME

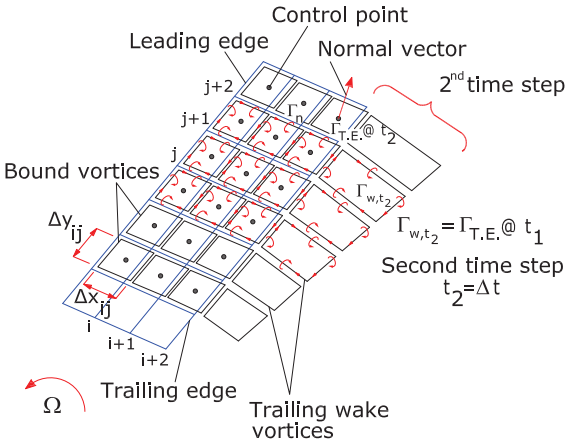

FIGURE 8. SCHEMATIC OF WAKE EVOLUTION AT THE SECOND TIME STEP

accuracy, stability and computational efficiency. Here, the first-order Euler explicit method is used as

$$\vec{r}_{t+1} = \vec{r}_t + \vec{V}(\vec{r}_t)\Delta t \tag{11}$$

where $\vec{V}$ is taken at the old time step.

Load Calculation

In the vortex flow, the only force acting on the rotor blades is the lift force which can be calculated either by the Kutta-Jukowski theory or the Bernoulli equation where the viscous effects such as the skin friction and the flow separation are not included. Therefore, in order to take into account the viscous effects and the flow separation, it must be combined with the aerodynamic coefficients through the tabulated airfoil data along with the dynamic stall model to model the unsteady effects.

The currently developed model is based on the thin lifting surface theory of vortex ring elements, where the body is part of the flow domain. Therefore, the effective angle of attack is calculated based on the dynamic approach (force field) by projecting the lift force acting on rotor blades into the normal and tangential directions with respect to the rotor plane. Since the predicted angle of attack, computed on the basis of the potential flow solution (i.e., the lifting surface theory), is always greater than that calculated by the viscous flow, it cannot be directly used as entry to look up the tabulated airfoil data to provide the aerodynamic coefficients.

In the standard potential method, the airfoil characteristic of each spanwise section is not taken into account. Therefore, in the 2D static airfoil data method, the new angle of attack is calculated by using the tabulated airfoil data where it is directly connected to the both tabulated airfoil data and the potential solution parameter (Γ). This angle of attack is used as the entry to look-up the airfoil table and then we are able to calculate the lift, drag and moment coefficients giving the lift and drag forces for each blade element. These two methods, the standard potential method and the 2D static airfoil data method, are based on the quasi-static assumption.

In the fully unsteady condition, since the lift, drag and moment coefficients are not following the tabulated airfoil data curve, as it was described in the introduction, they should be corrected and this is done by a dynamic stall model. Generally, the aim of the dynamic stall model is to correct the aerodynamic coefficients under the different time-dependent events which were described in the introduction. In case of uniform, steady inflow condition and in the absence of the blade aeroelastic motion, it is not necessary to use the dynamic stall model. However, it should be noted that even though in the steady state condition, the induced velocity field by the blade and the wake elements vary during the wake evolution, hence using the dynamic stall model for the load calculation is unavoidable.

The Standard Potential Method In the VLFW method, when the position of all the Lagrangian markers is calculated in each time step, we are able to compute the velocity field around the rotor blade where, as a consequence, the lift force can be calculated according to the Kutta-Jukowski theorem which in differential form reads as

$$\vec{dL} = \rho \vec{V} \times \Gamma \vec{dl} \tag{12}$$

where ρ, $\vec{V}$, Γ and $\vec{dl}$ denote air density, velocity vector, vortex filament strength and length vector, respectively. The Kutta-Jukowski theorem is applied at the mid-point of the front edge of each blade vortex ring and gives the potential lift force where the lift force of each spanwise blade section is calculated by summing up the lift force of all panels along the chord. The lift force for each blade panel except the first row near the leading edge is computed by

$$\vec{L}_{i,j} = \rho \vec{V}_{tot,i,j} \times (\Gamma_{i,j} - \Gamma_{i-1,j}) \Delta \vec{y}_{i,j} \tag{13}$$

For the blade panels adjacent to the leading edge, Eq.(13) can be written as

$$\vec{L}_{1,j} = \rho \vec{V}_{tot,1,j} \times \Gamma_{1,j} \Delta \vec{y}_{1,j} \tag{14}$$

where $\vec{V}_{tot,i,j}$ is computed as

$$\vec{V}_{tot,i,j} = \vec{V}_{und,i,j} + \vec{V}_{ind,wake,i,j} + \vec{V}_{ind,bound,i,j} \tag{15}$$

Copyright © 2014 by ASME

The total lift of each blade section in the spanwise direction is obtained as

$$\overrightarrow{L}_j = \sum_{i=1}^{N} \overrightarrow{L}_{i,j} \tag{16}$$

where N denotes the number of chordwise sections. Decomposition of the lift force for each blade spanwise section into the normal and tangential directions with respect to the rotor plane (see Fig.(9)) gives the effective potential angle of attack for each section.

$$\alpha = tan^{-1}(F_t/F_n) - \theta_t - \theta_p \tag{17}$$

where α, F_t, F_n, θ_t and θ_p represent the effective angle of attack, tangential force, normal force, blade section twist and blade pitch, respectively.

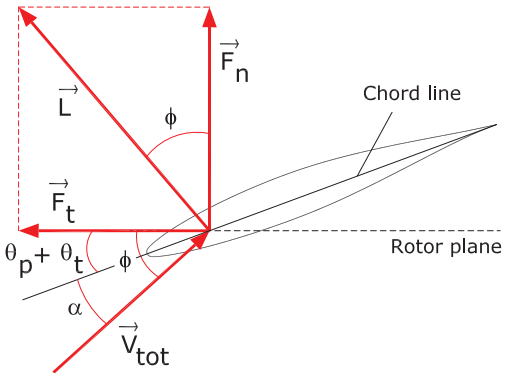

FIGURE 9. POTENTIAL LOAD DECOMPOSITION

2D Static Airfoil Data Method In the potential flow, the lift coefficient, expressed by the thin airfoil theory, is a linear function of angle of attack with constant slope equal to 2π. This means that for the thick airfoil, commonly used in wind turbine blades, the thin airfoil theory is not valid. In addition, because of this linear relation of the lift coefficient and the angle of attack, the higher the lift the higher the angle of attack. Hence, considerable lift reduction due to flow separation at higher angles of attack cannot be predicted.

According to the Kutta-Jukowski theory, the magnitude of the lift force per unit spanwise length, L', is proportional to the circulation, Γ, and it is given by

$$L' = \rho V_{tot} \Gamma \tag{18}$$

where ρ, V_{tot} denote the air density and the total velocity magnitude, respectively. The circulation for each spanwise section is equal to the bound vortex circulation of the last row vortex ring element, located at the trailing edge. In addition, in the linear airfoil theory, the lift coefficient is expressed by

$$C_L = m(\alpha - \alpha_0) \tag{19}$$

where $m = 2\pi$, α and α_0 indicate the slope, the angle of attack and the zero-lift angle of attack, respectively. The lift coefficient is generally defined as

$$C_L = \frac{L'}{0.5\rho V_{tot}^2 c} \tag{20}$$

where c denotes the airfoil chord length. Combination of Eqs.(18), (19) and (20) gives the modified angle of attack as

$$\alpha = \frac{2\Gamma}{m V_{tot} c} + \alpha_0 \tag{21}$$

For an arbitrary airfoil, both m and α_0 are determined according to the C_L vs. α curve where the constant lift coefficient slope, m, is computed over the linear region (attached flow). The modified angle of attack based on the Eq.(21) is used as entry to calculate the lift, the drag and the moment coefficients through the tabulated airfoil data. As a result, the lift and the drag forces are

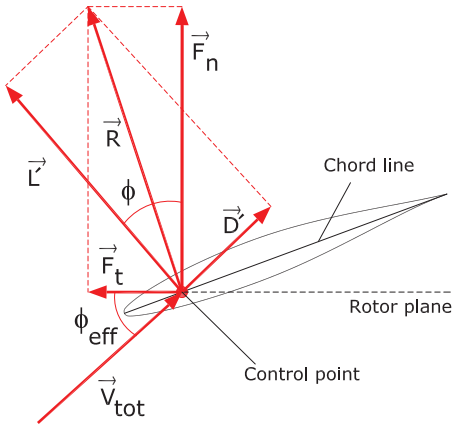

FIGURE 10. VISCOUS LOAD DECOMPOSITION

computed for each blade element in the spanwise section giving the tangential and the normal forces acting on the rotor blade (see Fig.(10)).

Copyright © 2014 by ASME

Dynamic Stall Method The semi-empirical dynamic stall model, called the Extended ONERA is used to predict the unsteady lift, drag and moment coefficients for each blade spanwise section based on 2D static airfoil data. In this model, the unsteady airfoil coefficients are described by a set of differential equations including the excitation and the response variables, where they are applied separately for both the attached and the separated flows.

In the initial version of the ONERA model, the excitation variable is the angle of attack with respect to the chord line whereas in the extended version, the excitation variables are W_0 and W_1, the velocity component perpendicular to the chord and the blade element angular velocity for the pitching oscillation, respectively.

Furthermore, compared with the initial version of ONERA model, in the extended model, instead of the lift coefficient (C_L), the circulation (Γ) which is responsible for producing lift is the response variable. Also, the variation of the wind velocity is included in the extended model which does not exist in the early version [9].

In the extended ONERA model, the lift (L) and the drag (D) forces are written as

$$L = \frac{\rho c}{2}\left[V_{tot}\left(\Gamma_{1L}+\Gamma_{2L}\right)+\frac{S_L c}{2}\dot{W}_0+\frac{K_L c}{2}\dot{W}_1\right] \qquad (22)$$

and

$$D = \frac{\rho c}{2}\left[V_{tot}^2 C_{D,Lin}+\frac{\sigma_D c}{2}\dot{W}_0+V_{tot}\Gamma_{2D}\right] \qquad (23)$$

where ρ, c, V_{tot}, Γ_{1L}, Γ_{2L}, W_0, W_1, Γ_{2D} and $C_{D,Lin}$ denote the air density, blade element chord length, total velocity, linear circulation related to the attached flow lift, non-linear circulation related to the separated flow lift, total velocity component perpendicular to the chord, blade section rotational velocity due to the pitching oscillation and non-linear circulation related to the separated flow drag and linear drag coefficient, respectively. For the detailed description of other coefficients in Eqs.(22) and (23), see appendix A.

RESULTS

The $5MW$ reference wind turbine [19] is used in the simulations. Table (1) shows the operating conditions in which the simulations have been done. In the vortex method simulations made with VLFW and GENUVP, the blade is discretized with $M = 25$ spanwise sections (see Fig.(11)) with fine tip resolution and $N = 8$ equally spaced chordwise sections. 10 degrees in the azimuthal direction is employed for the wake segmentation and the wake length is truncated after 4 rotor diameters. It is assumed that the wake vortex filament core radius is constant and is equal to $1[m]$. The free stream is assumed to be uniform, steady and perpendicular to the rotor plane. Moreover, all coefficients in the dynamic stall calculations are taken according to the flat plat and the mean profile values.

Case No.	V_∞ [m/s]	Ω [rad/s]	Pitch angle [deg]
1	5	0.627	0.0
2	6	0.753	0.0
3	7	0.878	0.0
4	8	1.003	0.0
5	9	1.129	0.0
6	10	1.255	0.0
7	11	1.267	0.0
8	12	1.267	4.0
9	13	1.267	6.65
10	14	1.267	8.70
11	15	1.267	10.46

TABLE 1. NREL TURBINE OPERATING CONDITIONS

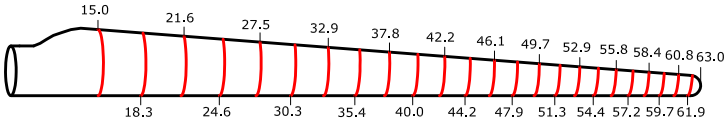

FIGURE 11. RADIAL DISTRIBUTION OF BLADE ELEMENTS

Figures (12), (13) and (14) show the effective angle of attack along the blade. As can be seen, the potential angle of attack is greater than the viscous one which is consistent with the higher power production, predicted by the potential solution. The blade of the $5MW$ NREL machine is constructed by the different airfoil profiles [19]. Computing the lift coefficient slope in the linear region (attached flow) for each airfoil profiles, shows that this slope is larger than the slope for the thin airfoil theory ($m = 2\pi$). By looking at Eq.(21), it is found out that the larger the lift coefficient slope (m), the lower the angle of attack. Therefore, the modification of the potential angle of attack by coupling to the 2D airfoil data influences the load and power predictions.

Figures (15), (16) and (17) show the tangential force along the blade with respect to the rotor plane. Three different solutions of the VLFW method are compared together. The predicted tangential force by the potential solution is significantly larger near

Copyright © 2014 by ASME

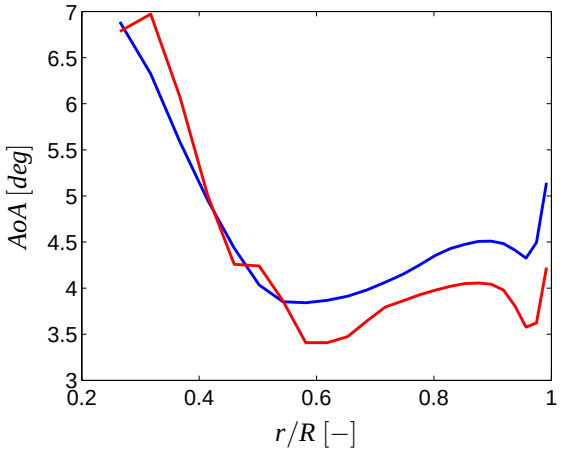

FIGURE 12. DISTRIBUTION OF THE ANGLE OF ATTACK ALONG THE BLADE FOR CASE 2, ——: *POTENTIAL*, ——: *VISCOUS*

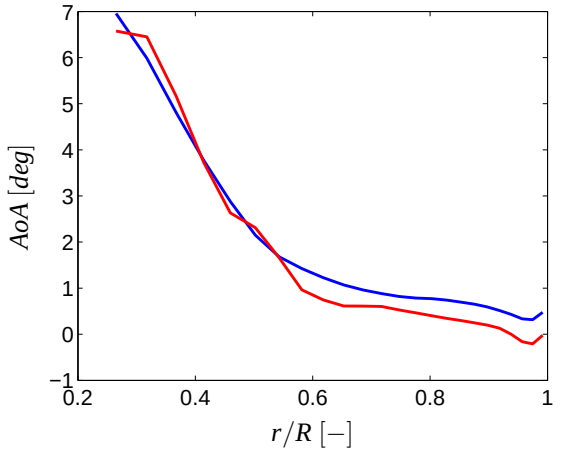

FIGURE 14. DISTRIBUTION OF THE ANGLE OF ATTACK ALONG THE BLADE FOR CASE 10, ——: *POTENTIAL*, ——: *VISCOUS*

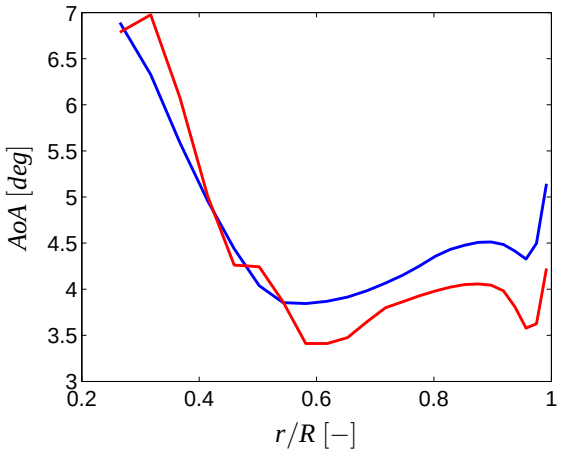

FIGURE 13. DISTRIBUTION OF THE ANGLE OF ATTACK ALONG THE BLADE FOR CASE 6, ——: *POTENTIAL*, ——: *VISCOUS*

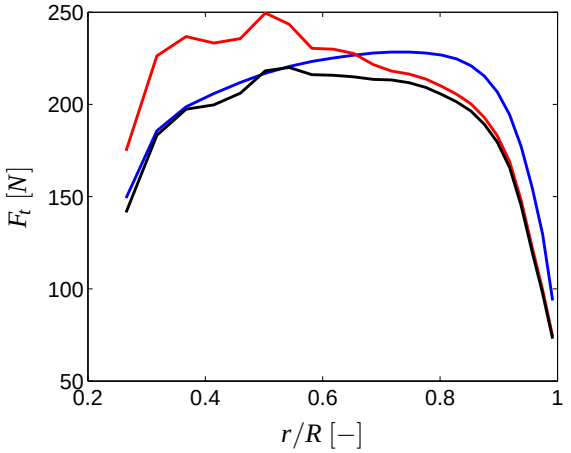

FIGURE 15. DISTRIBUTION OF THE TANGENTIAL FORCE ALONG THE BLADE FOR CASE 2, ——: *POTENTIAL*, ——: *VISCOUS*, ——: *DYNAMIC STALL*

the blade tip making more power in comparison with the viscous and the dynamic stall solutions. In addition, the tangential force calculated by the viscous solution gives larger values than the potential solution near the blade root region. The difference between the potential and the viscous solution for the tangential force, close to the blade root, considerably increases for the higher wind velocity where the turbine is pitch regulated to prevent the turbine operating above the rated power. The dynamic stall solution which modifies the aerodynamic coefficients due to the time variation of the total velocity and the effective angle of attack lies between the potential and the viscous solution, coincided with the viscous solution for half of the blade toward the blade tip and with the potential solution toward the blade root.

Figures (18) shows the power curve for the $5MW$ NREL turbine. For the attached flow region (no pitch regulation), where the wind velocity is less than the $11m/s$, the VLFW potential solution, predicts more power than the VLFW viscous solution, the VLFW dynamic stall solution and the BEM method. Also, for the wind velocity higher than $11m/s$ (pitch regulated zone) where the viscosity effect is significant, the potential solution predicts the less power than the viscous solution.

Figures (19) displays the thrust curve for the $5MW$ NREL turbine. By increasing the upstream flow, the wind turbine thrust linearly increases where it suddenly drops when the blade pitch angle is increased. The different methods approximately provide the equivalent results.

Copyright © 2014 by ASME

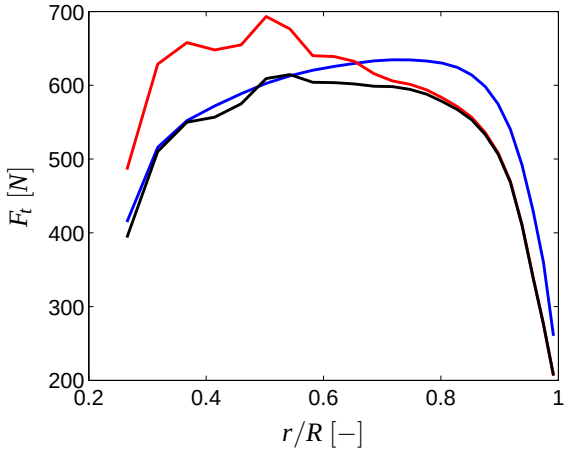

FIGURE 16. DISTRIBUTION OF THE TANGENTIAL FORCE ALONG THE BLADE FOR CASE 6, ——: *POTENTIAL*, ——: *VISCOUS*, ——: *DYNAMIC STALL*

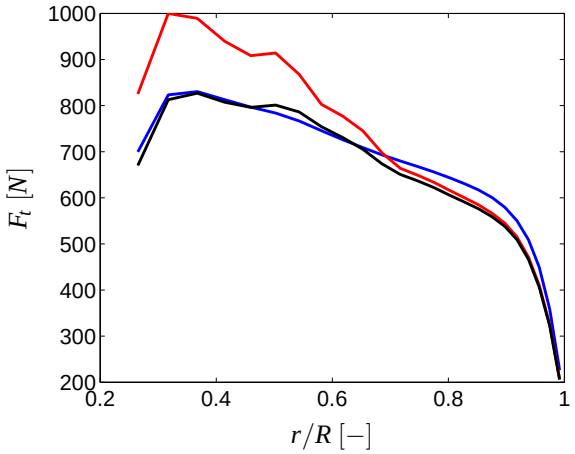

FIGURE 17. DISTRIBUTION OF THE TANGENTIAL FORCE ALONG THE BLADE FOR CASE 10, ——: *POTENTIAL*, ——: *VISCOUS*, ——: *DYNAMIC STALL*

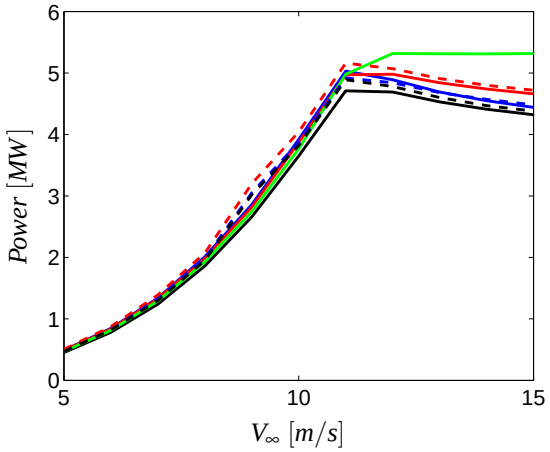

FIGURE 18. POWER CURVE FOR THE NREL TURBINE, ——: *VLFW POTENTIAL*, ——: *VLFW VISCOUS*, ——: *VLFW DYNAMIC STALL*, ——: *BEM*, - - - - - -: *GENUVP POTENTIAL*, - - - - - -: *GENUVP VISCOUS*, - - - - - -: *GENUVP DYNAMIC STALL*

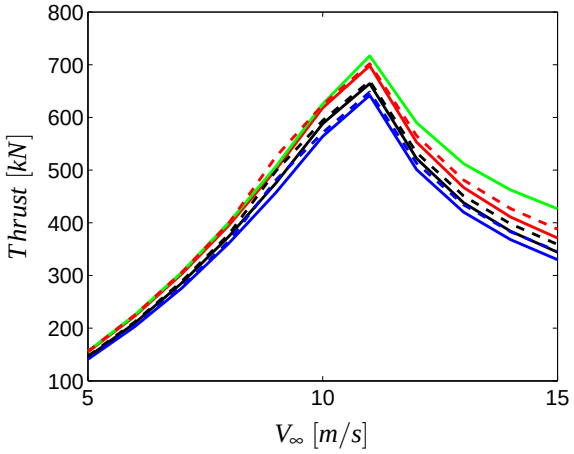

FIGURE 19. THRUST CURVE FOR THE NREL TURBINE, ——: *VLFW POTENTIAL*, ——: *VLFW VISCOUS*, ——: *VLFW DYNAMIC STALL*, ——: *BEM*, - - - - - -: *GENUVP POTENTIAL*, - - - - - -: *GENUVP VISCOUS*, - - - - - -: *GENUVP DYNAMIC STALL*

SUMMARY AND CONCLUSIONS

A time-marching vortex lattice free wake is used for prediction of aerodynamic loads on rotor blades. It is based on the potential, inviscid and irrotational flow where its potential solution is coupled to the tabulated airfoil data and a semi-empirical model to take into account the viscosity and the dynamic stall effects, respectively. Three different methods called the standard potential method, the 2D static airfoil data method and the dynamic stall method are introduced and they are compared with the Blade Element Momentum (BEM) [1] method and the GENUVP code [2]. The results show that for more accurate load and power prediction, coupling to the tabulated airfoil data seems to be necessary. Moreover, the small difference for the power production between the different methods, at low wind velocity, implies that the potential, inviscid and irrotational assumptions of the vortex flow are relevant. Finally, the dynamic stall method standing between the other load calculation methods represents the dynamic response of the blade load to the wake evolution in time.

Copyright © 2014 by ASME

ACKNOWLEDGMENT

The technical support of National Technical University of Athens (NTUA) to use the GENUVP is greatfully acknowledged. (GENUVP is an unsteady flow solver based on vortex blob approximations developed for rotor systems by National Technical University of Athens).

This paper is a part of the research project (Theme group 2-1) financed through the Swedish Wind Power Technology Centre (SWPTC). SWPTC's work is funded by the Swedish Energy Agency, by three academic and thirteen industrial partners. The Region Västra Götaland also contributes to the Centre through several collaboration projects.

REFERENCES

[1] Hansen, M. O., 2008. *Aerodynamics Of Wind Turbines*. 2nd edition, EarthScan.

[2] Voutsinas, S., 2006. "Vortex Methods In Aeronautics: How To Make Things Work". *International Journal of Computational Fluid Dynamics,* ***20***, pp. 3–18.

[3] Gupta, S., 2006. *Development Of A Time-Accurate Viscous Lagrangian Vortex Wake Model For Wind Turbine Applications*. University of Maryland, Department of Aerospace Engineering.

[4] Pesmajoglou, S., and Graham, J., 2000. "Prediction Of Aerodynamic Forces On Horizontal Axis Wind Turbines In Free Yaw And Turblence". *Journal of Wind Engineering and Industrial Aerodynamics,* ***86***, pp. 1–14.

[5] Chattot, J., 2007. "Helicoidal Vortex Model For Wind Turbine Aeroelastic Simulation". *Computers and Structures,* ***85***, pp. 1072–1079.

[6] Chattot, J., 2003. "Optimization Of Wind Turbines Using Helicoidal Vortex Model". *Journal of Solar Energy Engineering,* ***125***, pp. 418–424.

[7] Holierhoek, J., de Vaal, J., van Zuijlen, A., and Bijl, H., 2013. "Comparing Different Dynamic Stall Models". *Journal of Wind Energy,* ***16***, pp. 139–158.

[8] Leishman, J., 2002. "Challenges In Modeling The Unsteady Aerodynamics Of Wind Turbines". *21st ASME Wind Energy Symposium and the 40th AIAA Aerospace Sciences Meeting, Reno, NV,* ***0037***.

[9] Bierbooms, W., 1992. "A Comparison Between Unsteady Aerodynamic Models". *Journal of Wind Engineering and Industrial Aerodynamics,* ***39***, pp. 23–33.

[10] Reddy, T. S. R., and Kaza, K. R. V., January 1989. *Analysis of an Unswept Propfan Blade With a Semi empirical Dynamic Stall Model*. NASA Technical Memorandum 4083.

[11] Anderson, J., 2001. *Fundamentals Of Aerodynamics*, 3rd ed. McGraw-Hill.

[12] van Garrel, A., 2001. *Requirements For A Wind Turbine Aerodynamics Simulation Module*, 1st ed. ECN report, ECN-C-01-099.

[13] Leishman, J., and Bagai, M. J., 2002. "Free Vortex Filament Methods For The Analysis Of Helicopter Rotor Wakes". *Journal of Aircraft,* ***39***.

[14] Bhagwat, M., and Leishman, J., 2002. "Generalized Viscous Vortex Model For Application To Free-Vortex Wake and Aeroacoustic Calculations". In 58th Annual Forum and Technology Display of the American Helicopter Society International.

[15] Vasitas, G., Kozel, V., and Mih, W., 1991. "A Simpler Model For Concentrated Vortices". *Experiments in Fluids,* ***11***, pp. 73–76.

[16] Bagai, A., and Leishman, J., 1993. "Flow Visualization Of Compressible Vortex Structures Using Density Gradient Techniques". *Experiments in Fluids,* ***15***, pp. 431–442.

[17] van Garrel, A., August 2003. *Development Of A Wind Turbine Aerodynamics Simulation Module*. ECN report, ECN-C–03-079.

[18] Katz, J., and Plotkin, A., 2001. *Low-Speed Aerodynamics*, 2nd ed. Cambridge University Press.

[19] Jonkman, J., Butterfield, S., Musial, W., and Scott, G., 2009, NREL/TP-500-38060. *Definition Of A 5-MW Reference Wind Turbine For Offshore System Development*. National Renewable Energy Laboratory, Colorado, USA.

Appendix A: Extended ONERA Model

In Eqs.(22) and (23), S_L, K_L and σ_D are airfoil dependent coefficients. However, in case of no wind tunnel measurement data, the flat plate values are applied as $S_L = \pi$ and $K_L = \pi/2$ for small Mach number. The term σ_D is expressed by

$$\sigma_D = \sigma_{0D}\alpha + \sigma_{1D} \mid \Delta C_L \mid \tag{24}$$

where for the flat plate, $\sigma_{0D} = 0$ and $\sigma_{1D} = 0$. Moreover, $\Delta C_L = C_{L,Lin} - C_{L,Stat}$ where the *Lin* and *Stat* subscripts represent the linear region and the static condition, respectively (see Figs.(20) and (21)). The linear circulation concerning the attached flow lift (Γ_{1L}) is calculated by the first-order differential equation as

$$\dot{\Gamma}_{1L} + \lambda_L \frac{2V}{c}\dot{\Gamma}_{1L} = \lambda_L \frac{2V}{c}\left(\frac{dC_L}{d\alpha}\right)(W_0 - V\alpha_0) + \lambda_L \frac{2V}{c}\sigma_L W_1 + \left(\alpha_L\left(\frac{dC_L}{d\alpha}\right) + d_L\right)\dot{W}_0 + \alpha_L\sigma_L\dot{W}_1 \tag{25}$$

where V, $\dfrac{dC_L}{d\alpha}$ and α_0 are the total velocity component parallel to the airfoil chord, slope of the C_L vs. α curve in the linear region and the zero-lift angle of attack of each blade element, respectively.

Copyright © 2014 by ASME

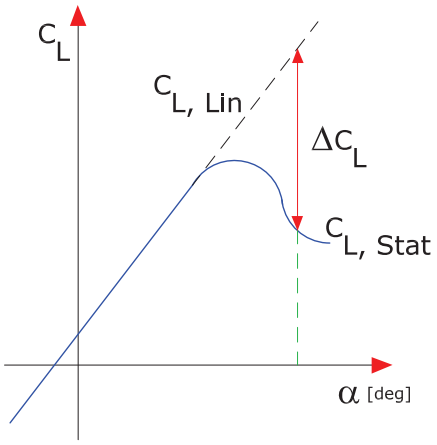

FIGURE 20. DEFINITION OF THE LIFT COEFFICIENT PARAMETERS IN THE ONERA MODEL

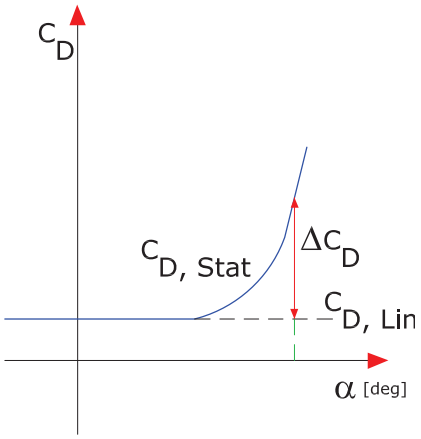

FIGURE 21. DEFINITION OF THE DRAG COEFFICIENT PARAMETERS IN THE ONERA MODEL

The non-linear circulation concerning the stall correction of lift (Γ_{2L}) is calculated by the second-order differential equation as

$$\ddot{\Gamma}_{2L}+a_L\frac{2V}{c}\dot{\Gamma}_{2L}+r_L\left(\frac{2V}{c}\right)^2\Gamma_{2L}=-r_L\left(\frac{2V}{c}\right)^2 V\Delta C_L-e_L\frac{2V}{c}\dot{W}_0 \tag{26}$$

Furthermore, the non-linear circulation concerning the stall correction of drag (Γ_{2L}) is given by the second-order differential equation as

$$\ddot{\Gamma}_{2D}+a_D\frac{2V}{c}\dot{\Gamma}_{2D}+r_D\left(\frac{2V}{c}\right)^2\Gamma_{2D}=-r_D\left(\frac{2V}{c}\right)^2 V\Delta C_D-e_D\frac{2V}{c}\dot{W}_0 \tag{27}$$

In Eqs.(22), (25), (26) and (27), the symbol $\dot{()}$ denotes the derivation with respect to the real time.

In the above equations, λ_L, σ_L and α_L depend on the specific airfoil type and they must be determined from the experimental measurements. If the experimental data for a particular airfoil is not available, these coefficients take the flat plate values as $\lambda_L = 0.17$, $\sigma_L = 2\pi$, $\alpha_L = 0.53$. d_L in Eq.(25) and the coefficients in Eqs.(26) and (27) are functions of ΔC_L due to the flow separation and they are defined as

$$\begin{aligned} d_L &= \sigma_{1L}\,|\,\Delta C_L\,| \\ a_L &= a_{0L}+a_{2L}(\Delta C_L)^2 \\ a_D &= a_{0D}+a_{2D}(\Delta C_L)^2 \\ \sqrt{r_L} &= r_{0L}+r_{2L}(\Delta C_L)^2 \\ \sqrt{r_D} &= r_{0D}+r_{2D}(\Delta C_L)^2 \\ e_L &= e_{2L}(\Delta C_L)^2 \\ e_D &= e_{2D}(\Delta C_L)^2 \end{aligned} \tag{28}$$

The coefficients in Eq.(28) are airfoil dependent. In case of no wind tunnel measurements, the values for a mean airfoil may be taken and the flat plate values cannot be used. For the mean airfoil, $\sigma_{1L} = 0.0$, $a_{0L} = 0.1$, $a_{2L} = 0.0$, $r_{0L} = 0.1$, $r_{2L} = 0.0$, $e_{2L} = 0.0$, $a_{0D} = 0.0$, $a_{2D} = 0.0$, $r_{0D} = 0.1$, $r_{2D} = 0.0$ and $e_{2D} = 0.0$.

Copyright © 2014 by ASME